

# Multigrid Implementation of Cellular Automata for Topology Optimization of Continuum Structures

R. Zakhama<sup>1,2,3</sup>, M.M. Abdalla<sup>2</sup>, H. Smaoui<sup>1,3</sup> and Z. Gürdal<sup>2</sup>

**Abstract:** A multigrid accelerated cellular automata algorithm for two and three dimensional continuum topology optimization problems is presented. The topology optimization problem is regularized using the traditional SIMP approach. The analysis rules are derived from the principle of minimum total potential energy, and the design rules are derived based on continuous optimality criteria interpreted as local Kuhn-Tucker conditions. Three versions of the algorithm are implemented; a cellular automata based design algorithm, a baseline multigrid algorithm for analysis acceleration and a full multigrid integrated analysis and design algorithm. It is shown that the multigrid accelerated cellular automata scheme is a powerful tool to solve topology optimization problems. This is demonstrated quantitatively by comparing the convergence time of the multigrid algorithm for different discretization levels, with that of the same design algorithm where the analysis is performed by a commercial finite element code.

**Keywords:** Topology optimization, Continuum structures, Multigrid, Cellular automata.

## 1 Introduction

In the last decade, research for more powerful tools to solve topology optimization problems in a practically reasonable computational time has achieved remarkable progress. Most commonly used approaches to solve the topology optimization problem are the homogenization approach [Bendsøe and Kikuchi (1988)], evolutionary methods [Xie and Steven (1993)] and the popular Simple Isotropic Material with Penalization (SIMP) approach [Bendsøe (1989); Juan, Shuyao, Yuanbo, and Guangyao (2008)]. More recently, a level set method [Wang and Wang (2006)] and a Cahn-Hilliard model (C-H) method Zhou and Wang (2006) have been pro-

---

<sup>1</sup> Civil Engineering, National School of Engineering at Tunis, Tunis, Tunisia.

<sup>2</sup> Aerospace Structures, Technical University of Delft, Delft, The Netherlands.

<sup>3</sup> LASMAP, Polytechnic School of Tunisia, La Marsa, Tunisia.

posed. Currently, there is a growing interest in topology design of complex 3D structures with massively parallel algorithms [Slotta, Tatting, Watson, Gürdal, and Missoum (2002); Setoodeh, Adams, Gürdal, and Watson (2006)]. Most available design algorithms are serial in nature, are based on global schemes and require a large number of costly analyses [Bendsøe and Kikuchi (1988); Bendsøe (1989)]. Nevertheless, there has been an increasing research effort to improve the computational efficiency for solving the topology optimization problems on serial machines [Cisilino (2006); Wang and Wang (2006); Zhou and Wang (2006)].

Wang and Wang (2006) proposed the level set approach based on an implicit free boundary parametrization method for structural shape and topology optimization problems. The implicit level set function is approximated using the Radial Basis Functions (RBFs). A steepest gradient method was used to find the descent direction of an auxiliary function that favors fast convergence of the minimization process.

The use of finite element methods within the topology optimization procedures leads in some cases to numerical instabilities, such as mesh-dependencies. Li and Atluri (2008b) proposed to use the The Meshless Local Petrov-Galerkin (MLPG) "mixed collocation" method to overcome the mesh-dependencies problem. These meshless methods have an advantage over the element-based approaches due to the elimination of the mesh. The MLPG "mixed collocation" method adopts the Moving Least Squares (MLS) interpolation to approximate the displacement function. The authors used the MLPG "mixed collocation" method to discretize the design domain. The optimization design variables were related to the nodes instead of the common used element design variables. The SIMP approach was selected and the Optimality Criteria (OC) method was employed to solve the topology optimization problem. The same authors Li and Atluri (2008a) extended their work to perform topology optimization of orthotropic composite structures.

Juan, Shuyao, Yuanbo, and Guangyao (2008) proposed to formulate the topology optimization problem based on the meshless Radial Point Interpolation Method (RPIM) and the SIMP approach. The major advantage of this method is to overcome the singularity problem of the meshless Point Interpolation Methods (PIM) proposed by Liu and Gu (2001) based on only polynomial basis function. The authors of this paper considered the relative density of nodes as a design variable to eliminate the checkerboard phenomenon. The adjoint method was used to formulate the sensitivities of the objective function and the volume constraint. Numerical examples demonstrated that this method can effectively eliminate the checkerboard phenomenon.

A methodology based on the Cellular Automata (CA) paradigm has been demonstrated to be efficient in solving this class of optimization problems [Kita and Toy-

oda (2000); Gürdal and Tatting (2000)]. The method has also been successfully implemented on both traditional and parallel hardware architectures [Gürdal and Tatting (2000); Slotta, Tatting, Watson, Gürdal, and Missoum (2002); Setoodeh, Adams, Gürdal, and Watson (2006)]. In this paper, the Multigrid (MG) scheme is proposed to accelerate the CA algorithm implemented on traditional hardware architecture. The motivation behind this coupling is that the cellular automata paradigm and the multigrid scheme are closely related in their nature.

The cellular automata paradigm is a mapping of discrete dynamic systems in time and space. Each cell of the discrete domain communicates only with its neighborhood through simple local rules of transition. These rules are functions of the states of the cell itself and its neighboring cells. Global convergence is sought by applying the local rules repetitively to the entire domain.

Kita and Toyoda (2000) were among the first to use the cellular automata paradigm for solving topology optimization problems. They constructed CA design rules to obtain two-dimensional topologies based on an Evolutionary Structural Optimization (ESO) approach [Xie and Steven (1993)], where the analysis of the structure is performed using the finite element method.

Another pioneering work is attributed to Gürdal and Tatting (2000) and Tatting and Gürdal (2003). Using the CA paradigm they performed the analysis and design tasks in an integrated scheme to solve the topology design problem. A Stress Ratio (SR) method was chosen for the design update rule. The method was applied to the topology design of trusses and two-dimensional continua modelled as equivalent trusses. It was also extended to design of beams [Abdalla and Gürdal (2002)], 2D linear isotropic continua [Abdalla and Gürdal (2004)], fibre-angle distribution of anisotropic laminae [Setoodeh, Abdalla, and Gürdal (2005)], and topology of geometrically nonlinear 2D elastic continua modelled as equivalent trusses [Zakhama, Abdalla, Smaoui, and Gürdal (2006)].

In these studies, it has been observed that the CA convergence rate deteriorates considerably as the grid is refined. This is due to the slow propagation of information across the domain. In addition, when a CA algorithm is implemented on a serial machine it loses its most attractive feature: parallelism. A methodology based on the multigrid scheme is proposed in this paper to accelerate the CA convergence process on serial machines. In earlier papers, it has been demonstrated that the CA method takes advantage of the acceleration effect of multigrid schemes [Kim, Abdalla, Gürdal, and Jones (2004); Zakhama, Abdalla, Smaoui, and Gürdal (2007)]. The main idea in the multigrid concept is to use different discretization levels of grids, where the iterations of a classical iterative method on the finer grid are coupled with the iterations for the correction of the solution on the coarser grids. This concept is illustrated in depth by Wesseling (1992). Hackbush (1985) presented

some applications of the multigrid algorithm such as solving elliptic partial differential equations and Poisson's equation.

In one of the earlier papers Maar and Schulz (2000) incorporated the multigrid method to accelerate the convergence of a nonlinear interior point algorithm applied to topology optimization problems. In [Kim and Yoon (2000)] the authors described the new concept of multi-resolution in multi-scale topology optimization. They formulated the design optimisation variable in a wavelet-based variable space, not in a direct density variable space. Using this method, major numerical instabilities such as mesh-dependencies and local minima are resolved. Dreyer, Maar, and Schulz (2000) presented two formulations of multigrid methods for optimization problems: the reduced SQP with multigrid solution of the linearized model equation and the simultaneous multigrids for solution of quadratic subproblems in a SQP-algorithm. Shape optimization of turbine blades and topology optimization of elastic structures are chosen as numerical examples for these two formulations. Kwon, Kim, Jang, and Kim (2002) incorporated the multigrid method into a multi-scale method to improve numerical efficiency. It is only in the work of Kim, Abdalla, Gürdal, and Jones (2004) and Zakhama, Abdalla, Smaoui, and Gürdal (2007) where the multigrid method was applied to accelerate the convergence of a cellular automata algorithm for structural design optimization, precisely of beam and 2D elastic continuum topology, respectively.

In the present paper, CA analysis update rules for two and three dimensional linearly elastic continua are derived from the principle of minimum total potential energy. The design rules are derived based on continuous optimality criteria interpreted as local Kuhn-Tucker conditions and regularized using the SIMP approach. The multigrid scheme is used to accelerate the cellular automata convergence. Numerical examples are presented to demonstrate the efficiency of the algorithm in solving topology optimization problems.

The rest of this paper is organized as follows. Formulation of the minimum compliance problem is given in Section 2. Cellular automata implementation is described in Section 3. In Section 4 the multigrid scheme is presented. Numerical examples are presented in Section 5 followed by conclusions in Section 6.

## 2 Formulation of the minimum compliance problem

The structural topology design problem is posed according to the minimal compliance formulation. Its aim is minimizing the elastic strain energy of the structure, or equivalently maximizing its total potential energy  $\Pi$  at equilibrium, subject to a limitation on the material volume. Thus, the design problem is written as

$$\min_{\rho} W_c(\rho, \mathbf{u}^*) \quad \text{or} \quad \max_{\rho} \Pi(\rho, \mathbf{u}^*), \quad (1)$$

under the constraints:

$$\mathbf{g}(\rho) \leq 0, \quad (2)$$

and the volume constraint:

$$\int_{\Omega} \rho \, d\Omega \leq \eta \cdot V_{\Omega}, \quad (3)$$

where  $\rho$  is the local density distribution of material which is chosen as the design variable,  $\Omega$  is the prescribed design domain,  $\mathbf{u}^*$  is the displacement vector at equilibrium, and  $\mathbf{g}$  is a vector of local constraints which set bounds on the density distribution. The volume  $V$  of the structure is limited to an available fraction  $\eta$  of the total volume of the design material domain. From the optimality conditions of the system level design problem (1)-(3), local optimality conditions are derived which are associated to the cell level optimization problem. According to the specialization of the SIMP method, the local stiffness of the structure is expressed as a function of a fictitious local density distribution  $\rho$ . The local optimization problem takes on the form [Abdalla and Gürdal (2002); Setoodeh, Abdalla, and Gürdal (2005)]:

$$\min_{\rho} \frac{\Phi^*(\sigma)}{\rho^p} + \mu \rho, \quad (4)$$

$$\varepsilon \leq \rho \leq 1, \quad (5)$$

where

- $\varepsilon > 0$  is a very small number, set as a lower bound on  $\rho$  to avoid numerical instability that may result from structural discontinuities when zero density is allowed,
- $p \geq 1$  is a penalization parameter that is introduced in order to lead the design to a black or white topology, by assigning sufficiently high values to  $p$ , typically  $p = 3$ ,
- $\Phi^* = \rho^p \hat{\Phi}$ , is an approximately invariant local quantity, and  $\hat{\Phi}$  is the complementary energy density,
- $\mu$  is the Lagrange multiplier associated with the global volume constraint (3).

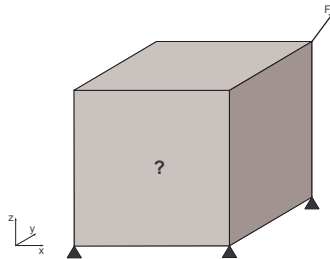
The solution of this one-dimensional convex problem is obtained analytically [Abdalla and Gürdal (2002); Setoodeh, Abdalla, and Gürdal (2005)] in the form:

$$\begin{cases} \hat{\rho} & \text{for } \varepsilon < \hat{\rho} < 1 \\ \varepsilon & \text{for } \hat{\rho} \leq \varepsilon, \\ 1 & \text{for } \hat{\rho} \geq 1 \end{cases} \quad (6)$$

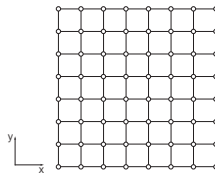
where

$$\hat{\rho} = \left( \frac{\Phi^*}{\bar{\mu}} \right)^{\frac{1}{1+p}}, \quad \bar{\mu} = \frac{\mu}{p}. \tag{7}$$

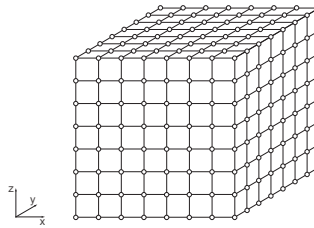
### 3 CA Implementation



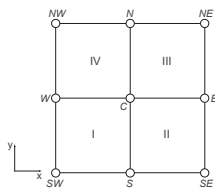
(a) Problem domain for topology design.



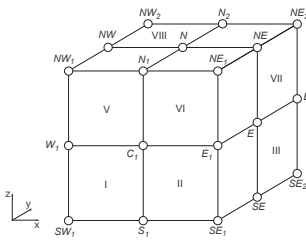
(b) 2D CA lattice.



(c) 3D CA lattice.



(d) 2D CA neighborhood.



(e) 3D CA neighborhood.

Figure 1: CA domain.

In the previous section, optimality based local rules for updating the material density were derived. In this section, the CA discretization of two and three dimensional structural domains is described. The elastic continuum domain (see

Fig. 1(a)) is discretized by a lattice of regular cells which are equally spaced in the  $x$  and  $y$  directions (see Fig. 1(b)), or  $x$ ,  $y$  and  $z$  for a three-dimensional structural domain (see Fig. 1(c)). Traditional Moore neighborhood is used to define the connectivity of the lattice as shown in Fig. 1(d) and 1(e). Each cell  $i$  communicates with its neighbors by a local rule and its state is denoted as  $\phi_i^k$  where  $k$  is the iteration number. For topology design in two and three dimensions, the state of the  $i^{\text{th}}$  cell is defined as

$$\phi_i = \{(u_{i(1,\dots,m)}), (f_{i(1,\dots,m)}), \rho_i\}, \quad (8)$$

where  $m$  corresponds the dimensionality of the domain,  $m = 2$  or  $3$  for two or three dimensions, respectively. The components  $(u_{i(1,\dots,m)})$  are the cell displacements in the directions  $(1, \dots, m)$ ,  $(f_{i(1,\dots,m)})$  the external forces acting on the  $i^{\text{th}}$  cell in the respective  $(1..m)$  directions. Each cell of the discretized domain has its own density measure  $\rho_i$  at the node point independently of the densities of the elements that define the neighborhood.

The update of the cells can be done simultaneously, which corresponds to the Jacobi scheme, as follows:

$$\phi_C^{k+1} = f(\phi_C^k, \phi_{NM}^k), \quad (9)$$

or sequentially, which corresponds to Gauss-Seidel scheme:

$$\phi_C^{k+1} = f(\phi_C^k, \phi_M^{k+1}, \phi_{NM}^k), \quad (10)$$

where  $M$  is the set of neighboring cells whose states have been modified in the current iteration and  $NM$  is the set of remaining cells, which have not yet been modified.

The Gauss-Seidel method is used for the analysis update. For the design update, the Jacobi method is the appropriate one to use to preserve the symmetry of the solution [Abdalla and Gürdal (2002)].

### 3.1 Analysis update rule

The local analysis rule is derived from the equilibrium condition of the cell. Within a cell, each element of the neighborhood structure has a Young modulus  $E$ . The total potential energy associated with a cell is the sum of the strain energy in each element of the neighborhood structure, added to the potential energy due to the external forces applied directly to the cell:

$$\Pi_i = \sum_{k=1}^{N_{element}} U_{i_k} - \mathbf{f}_i \cdot \mathbf{u}_i, \quad (11)$$

where  $N_{element}$  is the number of elements surrounding a cell,  $U_{i_k}$  is the strain energy for the  $k^{th}$  element,  $\mathbf{f}_i$  is the vector of applied forces and  $\mathbf{u}_i$  is the displacement vector for all the cell's neighborhood including the cell itself.

The strain energy of an element is expressed in terms of the strain energy of the base material as follows:

$$U_k = \bar{\rho}^p \tilde{U}, \quad (12)$$

where

$$\tilde{U} = \frac{1}{2} \int_{element} \Gamma \cdot \mathbf{Q} \cdot \Gamma \, dx dy dz \quad (13)$$

is the strain energy of the base material,  $\Gamma$  is the small-strain tensor, and  $\mathbf{Q}$  is the reduced inplane stiffness for isotropic materials. The element density  $\bar{\rho}$  are obtained by an average density interpolation [Abdalla and Gürdal (2002)] given by

$$\frac{1}{\bar{\rho}^p} = \frac{1}{N_{cell}} \sum_{i=1}^{N_{cell}} \frac{1}{\rho_i^p}, \quad (14)$$

where  $\rho_i$ 's are the density measures of the cells surrounding the element, and  $N_{cell}$  is the number of cells defining the element. For the two-dimensional neighborhood structure  $N_{cell} = 4$  and for the three-dimensional neighborhood structure  $N_{cell} = 8$ . It can be noted that since the compliance is inversely proportional to  $\rho^p$  (which measures the local stiffness), this scheme effectively assigns to each element an average value of the compliance values at the four cells.

This compliance averaging interpolation scheme is chosen so that any cell with a density measure below the threshold value  $\varepsilon$  would turn-off (force the assigned density to zero) all the elements in which that cell participates. This makes cells in white (void) regions have negligible or no effect on the equilibrium equations of cells in the black regions. Using this scheme, checkerboard patterns are suppressed automatically during the optimization process.

Thus, the equilibrium equations are obtained by minimizing the total potential energy with respect to the cell displacements:

$$\min_{\mathbf{u}_c} \Pi_i. \quad (15)$$

The resulting equilibrium equations for each cell are written in a residual form as

$$\mathbf{R}(\mathbf{u}_C, \mathbf{u}_N) = \left\{ \begin{array}{c} \mathbf{G}_C(\mathbf{u}_C, \mathbf{u}_N) \\ \mathbf{G}_N(\mathbf{u}_C, \mathbf{u}_N) \end{array} \right\} + \left\{ \begin{array}{c} \mathbf{f}_C \\ \mathbf{f}_N \end{array} \right\} = 0, \quad (16)$$



where  $\mathbf{u}_C$  and  $\mathbf{u}_N$  are the displacement vectors of the cell and the neighborhood, respectively,  $\mathbf{G}_C$  and  $\mathbf{G}_N$  are the vectors of the internal forces,  $\mathbf{f}_C$  and  $\mathbf{f}_N$  are the vector of the applied forces relative to the cell and the vector of the internal forces relative to the neighborhood, respectively.

Differentiating the vector  $\mathbf{R}$  with respect to the components of  $\mathbf{u}_C$ , the linear stiffness matrix can be written as

$$\mathbf{K} = -\frac{\partial \mathbf{R}}{\partial \mathbf{u}_C}(\mathbf{u}_C, \mathbf{u}_N). \quad (17)$$

The stiffness matrix  $\mathbf{K}$  can also be expressed as the Hessian of the total potential energy:

$$\mathbf{K}_{pq} = \frac{\partial^2 \Pi_i}{\partial u_p \partial u_q}. \quad (18)$$

Thus, the cell displacements are updated as follows:

$$\mathbf{u}_C^{t+1} = \mathbf{u}_C^t + \Delta \mathbf{u}_C, \quad (19)$$

$$\Delta \mathbf{u}_C = (\mathbf{K}_C)^{-1} \cdot (\mathbf{G}_C + \mathbf{f}_C), \quad (20)$$

where  $\mathbf{K}_C$  is the cell stiffness matrix,  $\mathbf{K}_C$  is a  $(2 \times 2)$  or  $(3 \times 3)$  matrix for the two or three dimensional case, respectively.

### 3.2 Design update

Cell densities are updated using (6). To this end, the cell strain energy density  $\Phi_c^*$  is calculated by averaging over cell neighborhood. Since the CA algorithm should handle finite domains, some cells will have shadow neighbors that lie outside the computational domain. Shadow cells are treated by setting their density  $\rho$  to zero. Due to the density interpolation scheme given by Eq. (14), these cells are automatically ignored from the solution. The area of the elements corresponding to shadow cells is not considered in averaging. In summary, the cell strain energy density  $\Phi_c^*$  is obtained as

$$\Phi_c^* = \frac{1}{n V_C} \sum_I^{N_{element}} \bar{\rho}_i^{2p} \tilde{U}_i, \quad (21)$$

where  $n$  is the number of elements with nonzero density,  $V_C$  is the volume of a cell,  $V_C = h^2$  or  $h^3$  for the two or three dimensional case, respectively, and  $h$  is the distance between two immediate neighbor cells.

### 3.3 Lagrange Multiplier Update

The proposed solution algorithm is of the primal-dual type. Therefore, the Lagrange multiplier associated with the volume constraint plays a central role in the iterative process (see Fig. 2). In each iteration its value  $\bar{\mu}$  is modified according to a simple update rule derived using Newton's method. Defining  $\mathcal{L}$  as the Lagrange function associated with the design optimization problem (1)-(3), the volume constraint is obtained by setting to zero the derivative of the Lagrangian function with respect to  $\bar{\mu}$ :

$$\frac{\partial \mathcal{L}}{\partial \bar{\mu}} = 0. \quad (22)$$

The volume constraint, Eq. (3), is approximated as

$$\sum_{cells} \rho_c V_c - \eta \sum_{cells} V_c = 0, \quad (23)$$

where  $V_c$  is the volume of a cell.

Although there are several iterative methods to solve Eq. (22), the Newton-Raphson method is chosen to solve it, due to its quadratic convergence. Thus, the update rule of the Lagrange multiplier, based on the solution given by (6), is as follows:

$$\bar{\mu}^{k+1} = \bar{\mu}^k + \Delta \bar{\mu}, \quad (24)$$

where

$$\Delta \bar{\mu} = -\frac{\frac{\partial \mathcal{L}}{\partial \bar{\mu}}}{\frac{\partial^2 \mathcal{L}}{\partial \bar{\mu}^2}}. \quad (25)$$

### 3.4 Cellular automata scheme

In this paper, the analysis and design iterations are nested. A flowchart of the CA design algorithm is presented in Fig. 2. Starting from a structure with zero displacements and from densities set to volume fraction  $\eta$ , analysis updates are performed repeatedly until the norm of the force imbalance (residual) reaches a pre-specified tolerance  $\varepsilon_r$ . Next, the design is updated over the whole domain, then the volume constraint is checked. If the volume constraint is not satisfied, the Lagrange multipliers are updated and so is the design. The process continues until the relative difference between five successive compliance values is less than a pre-specified tolerance  $\varepsilon_c$  and the variation in cell densities is less than a tolerance  $\varepsilon_d$ .

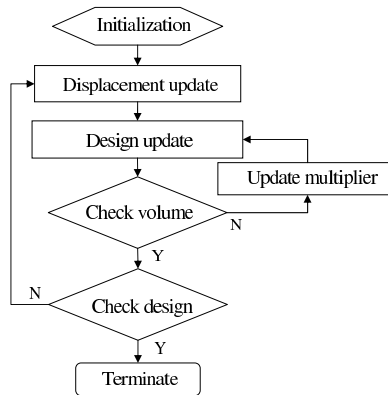


Figure 2: CA design algorithm.

From a computational perspective, the attractive feature of CA is its inherent parallelism. This feature appears to be particularly effective with regard to the analysis update. When it is not fully exploited, CA algorithms can be quite slow to converge. This is because communication between cells is limited only to immediate neighbors. The information from the cells where the loads are applied has to travel by neighbor-to-neighbor interaction throughout the domain. As the lattice is refined, the number of lattice updates needed to reach equilibrium significantly increases manifesting the deterioration in the rate of convergence alluded to above. Thus, when CA is implemented on a serial machine it loses its most attractive feature as far as the analysis update is concerned. The design features of CA, though, remain effective.

## 4 Multigrid implementation

### 4.1 Idea of multigrid

The convergence rate of a classical iterative schemes, such as Gauss-Seidel and Jacobi, for solving linear systems deteriorates considerably as the number of variables increases. The iteration of these schemes acts with the greatest efficiency on propagation/convergence of short wavelength, high frequency elements of the field information, while it is the components of low frequency information which persist that destroy the rate of convergence. In order to improve the performance of an iterative procedure, an initial approximation of the solution can be used, for example, by relaxation on a coarse grid using a classical iterative method. Since the variables on a coarse grid are fewer, the low frequency components of the field

information can be reduced without losing much precision and the computational cost for one relaxation is also much smaller than that on the fine grid. This relaxation method can then be used in order to obtain a better approximation for the finest grid solution.

The basic idea underlying the multigrid implementation is to use different discretization levels of grids; where the iterations of the classical iterative method (or the CA analysis method presented in this work) on the finest grid are coupled with the iterations of the correction solution on the coarser grids. It is well known that the classical iterative methods act directly on the high frequency components in the error  $\mathbf{e} = \mathbf{u} - \mathbf{v}$  of an approximation  $\mathbf{v}$  for the solution  $\mathbf{u}$  of the equation  $\mathbf{A}\mathbf{u} = \mathbf{b}$ . The error  $\mathbf{e}$  which is obtained from the residual equation  $\mathbf{A}\mathbf{e} = \mathbf{r}$  can be eliminated after a few iterations on the finest grid. However, after few iterations on the finest grid the convergence rate deteriorates due to the low frequency components. By using the relaxation scheme on a coarse grid in order to get an approximation to the error  $\mathbf{e}$  which corrects the fine grid approximation solution, the low frequency components will be eliminated. The coarse grid correction scheme is defined as follows:

- Relax on  $\mathbf{A}\mathbf{u} = \mathbf{b}$  on  $\Omega^k$  in order to obtain  $\mathbf{v}^k$ , where  $\Omega^k$  is a grid finer than  $\Omega^{k-1}$ .
- Compute the residual  $\mathbf{r} = \mathbf{b} - \mathbf{A}\mathbf{v}^k$ .
- Relax on  $\mathbf{A}\mathbf{e} = \mathbf{r}$  on  $\Omega^{k-1}$  to obtain an approximation to the error  $\mathbf{e}^{k-1}$ .
- Correct the approximation obtained on  $\Omega^k$  with the error estimate on  $\Omega^{k-1}$  by  $\mathbf{v}^k = \mathbf{v}^k + \mathbf{e}^{k-1}$ .

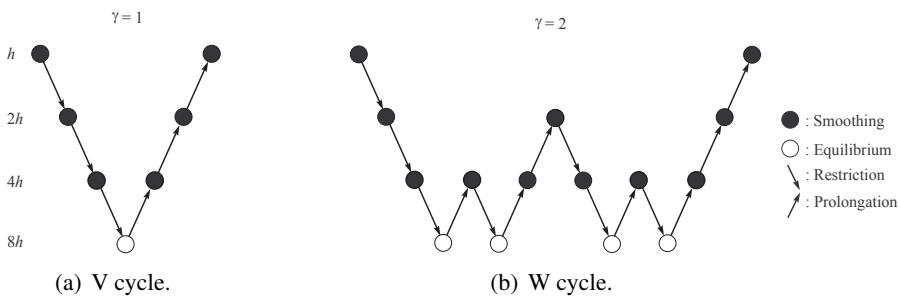


Figure 3: Multigrid strategies.

In this work, the multigrid scheme is used to accelerate the CA convergence for two and three dimensional topology optimization problems. The main difference between the MG design algorithm described in this work and the CA design algorithm described earlier is the acceleration of the analysis convergence. The strategies most used to visit the different grids are the **V** and **W** cycles [Wesseling (1992)]. Fig. 3 shows the order in which the grids are visited. A parameter  $\gamma_k$  represents the number of visiting times to a grid,  $\gamma_k = 1$  is assigned for the **V** cycle and  $\gamma_k = 2$  is assigned for the **W** cycle, respectively. A dot filled circle is used to represent a smoothing operation.

#### 4.2 Transfer operators

The relaxation scheme, also called multigrid scheme, is based on transformation operators between coarse and fine grids. Two operators, called prolongation and restriction operators, define the multigrid scheme. The prolongation, or interpolation, operator denoted by  $\mathbf{I}_{k-1}^k$  transforms functions from coarse grid  $\Omega^{k-1}$  to a fine grid  $\Omega^k$ . It maps the error  $\mathbf{e}^{k-1}$  obtained from the coarse grid  $\Omega^{k-1}$  onto the fine grid  $\Omega^k$ . The restriction operator, denoted by  $\mathbf{I}_k^{k-1}$ , is needed for transferring residual  $\mathbf{r}^k = \mathbf{b} - \mathbf{A}\mathbf{v}^k$  from a fine grid  $\Omega^k$  to a coarse grid  $\Omega^{k-1}$ .

In this paper, the prolongation and the restriction operators for the displacement fields are obtained by using bilinear interpolation between two generic grids  $\Omega^{k-1}$  and  $\Omega^k$ . In particular, the prolongation operator maps corrections  $\mathbf{e}$  of a solution in a coarse grid onto a fine grid as

$$\mathbf{e}^h = \mathbf{I}_{2h}^h \mathbf{e}^{2h}, \quad (26)$$

where the superscript  $h$  indicates the fine grid and  $2h$  indicates the coarse one. The prolongation operator for a two dimensional grid is illustrated in Fig. 4. The

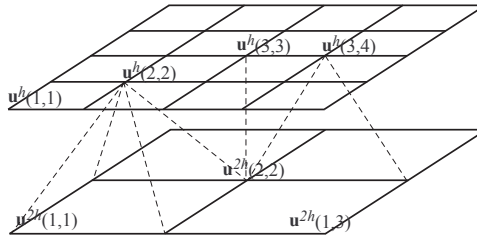


Figure 4: Two-dimensional prolongation.

correction of a cell on a coarse grid is projected unchanged onto a matching cell on

a fine grid as

$$\mathbf{u}^h(3,3) = \mathbf{u}^{2h}(2,2), \quad (27)$$

where  $\mathbf{u}$  represents the displacement vector of a cell.

The corrections of a fine grid cell which belongs to an edge of a coarse grid element are approximated as

$$\mathbf{u}^h(3,4) = \frac{1}{2} \left[ \mathbf{u}^{2h}(2,2) + \mathbf{u}^{2h}(2,3) \right]. \quad (28)$$

The corrections of a fine grid cell which is located at the middle of a coarse element are approximated using bilinear interpolation as

$$\mathbf{u}^h(2,2) = \frac{1}{4} \left[ \mathbf{u}^{2h}(1,1) + \mathbf{u}^{2h}(2,2) + \mathbf{u}^{2h}(2,1) + \mathbf{u}^{2h}(1,2) \right]. \quad (29)$$

Thus, the prolongation operator can be written in stencil notation as

$$\mathbf{I}_{2h}^h = \begin{bmatrix} \frac{1}{4} & \frac{1}{2} & \frac{1}{4} \\ \frac{1}{2} & 1 & \frac{1}{2} \\ \frac{1}{4} & \frac{1}{2} & \frac{1}{4} \end{bmatrix}. \quad (30)$$

Similarly, the prolongation operator in three-dimensions is obtained and can be written in stencil notation as follows:

$$\mathbf{I}_{2h}^{h(-1)} = \begin{bmatrix} \frac{1}{8} & \frac{1}{4} & \frac{1}{8} \\ \frac{1}{4} & \frac{1}{2} & \frac{1}{4} \\ \frac{1}{8} & \frac{1}{4} & \frac{1}{8} \end{bmatrix}, \quad \mathbf{I}_{2h}^{h(0)} = \begin{bmatrix} \frac{1}{4} & \frac{1}{2} & \frac{1}{4} \\ \frac{1}{2} & 1 & \frac{1}{2} \\ \frac{1}{4} & \frac{1}{2} & \frac{1}{4} \end{bmatrix},$$

$$\mathbf{I}_{2h}^{h(1)} = \begin{bmatrix} \frac{1}{8} & \frac{1}{4} & \frac{1}{8} \\ \frac{1}{4} & \frac{1}{2} & \frac{1}{4} \\ \frac{1}{8} & \frac{1}{4} & \frac{1}{8} \end{bmatrix}, \quad (31)$$

where the superscript  $(-1)$ ,  $(0)$  or  $(1)$  refers to the position of the matrix in the three-dimensional stencil  $\mathbf{I}_{2h}^h$ .

The restriction operator is needed or transferring the residual from a fine grid to a coarse grid as

$$\mathbf{r}^{2h} = \mathbf{I}_h^{2h} \mathbf{r}^h. \quad (32)$$

By means of Galerkin's approximation, the restriction operator is defined by

$$\mathbf{I}_h^{2h} = \left( \mathbf{I}_{2h}^h \right)^T. \quad (33)$$

However, the design is only performed on the finest grid. Then, the density in the fine grid is transformed by restriction to that in the coarse grid. For a two-dimensional problem, the density of each element in a coarse grid is determined by averaging the densities of the matching four elements in the finer grid:

$$\bar{\rho}_{2h}^p = \frac{1}{4} \sum_{i=1}^4 \bar{\rho}_{i_h}^p, \quad (34)$$

For a three-dimensional case, the density for an element in a coarse grid is obtained as

$$\bar{\rho}_{2h}^p = \frac{1}{8} \sum_{i=1}^8 \bar{\rho}_{i_h}^p. \quad (35)$$

### 4.3 Multigrid design algorithm

The multigrid design algorithm is very similar to the CA design algorithm described earlier. The main difference is that in the former the structural analysis update is implemented according to a multigrid enhanced CA method instead of the base CA method. The multigrid algorithm starts from the finest grid and visits all the hierarchy of coarse grids. Starting from a fine grid  $\Omega^h$ , the CA analysis update is applied  $\eta_1$  pre-relaxations times. The residual  $\mathbf{r}$  obtained from a fine grid  $\Omega^h$  is then mapped onto a coarse grid using the restriction operator  $\mathbf{I}_{2h}^h$ . The density of each element in a coarse grid is also restricted using Eq. (34) (resp. Eq. (35)) for a two-dimensional (resp. three-dimensional) problem. Arriving to the coarsest grid, the CA analysis update is executed until the residual ratio reaches a pre-specified tolerance or an exact solution is obtained if possible. Next, the corrections obtained from a coarse grid  $\Omega^{2h}$  are mapped onto a fine grid  $\Omega^h$  using the prolongation operator  $\mathbf{I}_h^{2h}$  followed by  $\eta_2$  post-relaxations. This scheme is repeated until the residual ratio reaches a pre-specified tolerance.

### 4.4 Full multigrid design algorithm

The idea behind the full multigrid (FMG) algorithm is to use an initial approximation to the solution of analysis and design for each given grid level in order to accelerate the convergence process. Starting from the coarsest grid ( $k = 1$ ) which requires less computational time to converge, the displacements and the design variables are interpolated recursively to a fine grid using the prolongation operator  $\mathbf{I}_h^{2h}$ . At a given fine grid in the FMG algorithm, the multigrid scheme and the design update rule are applied, whereas in the MG algorithm the design process is carried out only at the finest grid level (see Fig. 5).

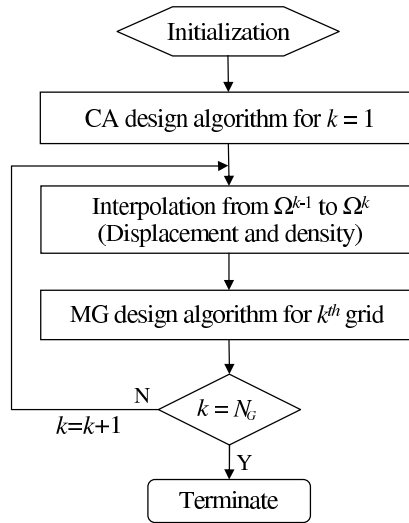


Figure 5: FMG design algorithm.

## 5 Numerical examples


















In this section, some examples of topology optimization are considered and the efficiency of the multigrid accelerated algorithm is examined. All algorithms described in this paper are implemented under a Linux C++ environment and tested on a Dual core AMD Opteron(tm) machine with a processor frequency of 2400 Mhz and 8 GByte memory. In all runs, the penalization parameter is set to 3. The tolerance for the compliance and the design is set to 0.1 and 0.05, respectively, and a lower bound of  $10^{-3}$  is adopted for the density. The tolerance for the residual ratio is set to 0.1 and 0.5 for the finest and the coarsest grids, respectively.

### 5.1 Example 1

In order to demonstrate the efficiency of the multigrid accelerated CA algorithm in solving the topology optimization problem, it is compared with existing methods. Since the same CA design update rule is used in all tested algorithms, the comparison concerns design algorithms based on different analysis processes, namely the different multigrid schemes and the commercial NASTRAN code. The example studied is a symmetric cantilever with 1000 mm in length, 250 mm in height and 1 mm in thickness. The volume fraction is set to 0.5, the tip load considered is  $P = 100$  N, the Poisson ratio is 0.4 and the Young modulus  $E$  used is  $1000$  N/mm<sup>2</sup>.



Table 1: Optimal topologies and compliances.

Cell number	Optimal topology using NASTRAN	Optimal topology using MG	Optimal topology using FMG
$129 \times 33$	 4273.6	 4258.7	 4189.3
$257 \times 65$	 4064.1	 4062.7	 3859.6
$513 \times 129$	 3985.7	 3984.2	 3727.9
$1025 \times 257$	 3983	 3980.9	 3668.8
$2049 \times 513$	 3994	 3992	 3642
$4097 \times 1025$	lack of memory	 3998.4	 3634.3

Different discretization levels are used for the comparison; the results are generated for 11 grid levels, starting from the coarsest grid level of  $9 \times 3$  cells, up to the finest grid level of  $4097 \times 1025$  cells. The W-cycle is used for the multigrid process. Convergence time for the FEM-CA solution using the commercial NASTRAN code and for both the multigrid accelerated CA algorithm and the full multigrid design algorithm are illustrated in Fig. 6. The vertical and horizontal axes represent the convergence time and the number of cells, respectively, on a log-log scale. First, it is observed that the curves corresponding to the MG accelerated CA algorithm and the FMG design algorithm have approximately the same slope with a small time gain for the FMG algorithm when the number of variables is large enough. The plot given when using the commercial NASTRAN code showed a higher convergence time than the other two algorithms. Moreover, the commercial NASTRAN code suffers lack of memory while running the grid level of  $4097 \times 1025$  cells. On the contrary, the cellular automata paradigm can handle large problems because of its local nature which makes the storage of the global stiffness matrix unnecessary. The run time to convergence relative to the MG and FMG algorithms appears to be

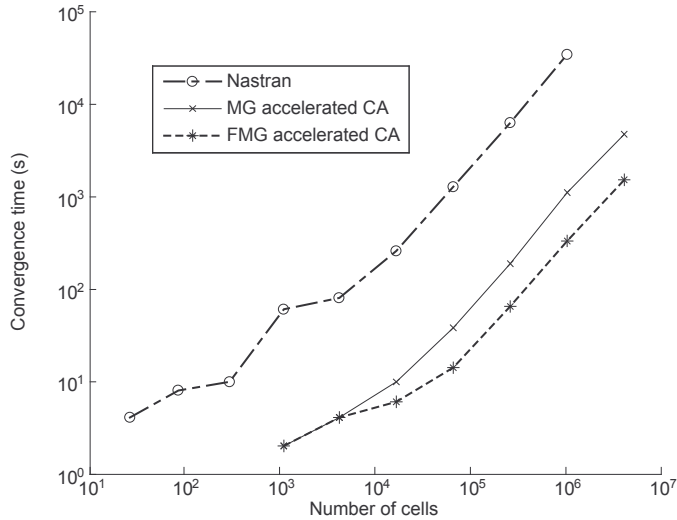


Figure 6: Convergence time using NASTRAN, MG accelerated CA and FMG.

nearly proportional to the number of cells, which reveals a computational effort in the order of  $O(N)$ . As for the optimal topologies, from Tab. 1 it can be seen that those obtained by the MG algorithm and by the use of NASTRAN for analysis are practically the same with a slightly (0.005% to 0.03%) but persistently lower compliance in the MG results. The FMG algorithm, however, produces a remarkably distinct topology, with a gain between 2% and 9% in compliance, compared to the topologies given by the former algorithms. This performance is mainly attributed to the fact that the FMG algorithm starts successively from a better design as the grid level goes up.

## 5.2 Example 2

In this example, the objective is to find an optimal topology for a bridge which crosses a river and supports a uniformly distributed traffic loading. The design domain, the loading and the boundary conditions of the bridge problem are represented in Fig. 7. Requirements of waterway traffic underneath and road traffic on the bridge translate into the definition of imposed zones: an empty (white) zone for the waterway and a dense (black) one for the deck, as represented in Fig. 7. The design domain is discretized with  $257 \times 65$  cells for the two-dimensional case and with  $257 \times 65 \times 33$  for the three-dimensional case including the empty zone. The volume fraction is set to 0.1 and the Poisson ratio to 0.3.

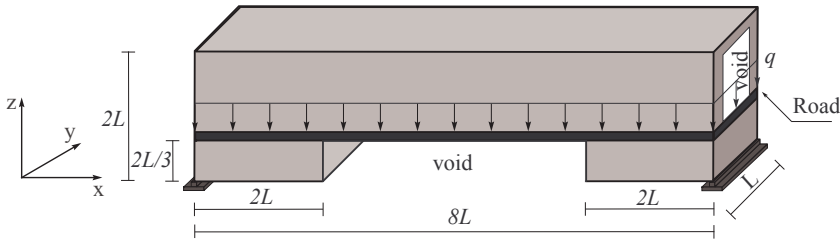


Figure 7: Compression bridge domain.

The final topology for the two-dimensional case performed by the MG design



Figure 8: Optimal 2D topology of compression bridge.

algorithm is represented in Fig. 8. It corresponds to a compression arch which holds a three span deck. The first and the third spans are cantilevers which are supported each by a compression member, whereas the central span is suspended via a series of tension members. Different views for the three-dimensional version of the topology of the bridge are shown in Fig. 9. The topology obtained with the three-dimensional model presents some similarity, in the XZ plane, with the topology generated by the two-dimensional model (see Fig. 9(a) and 8) and with the design of the compression arch bridge reported in [Beckers (1999)]. The algorithm for two-dimensional case converges in a total of 57 design updates in about 30 seconds, and for the three-dimensional case converges in a total of 56 design updates and the run time is about 7973 seconds.

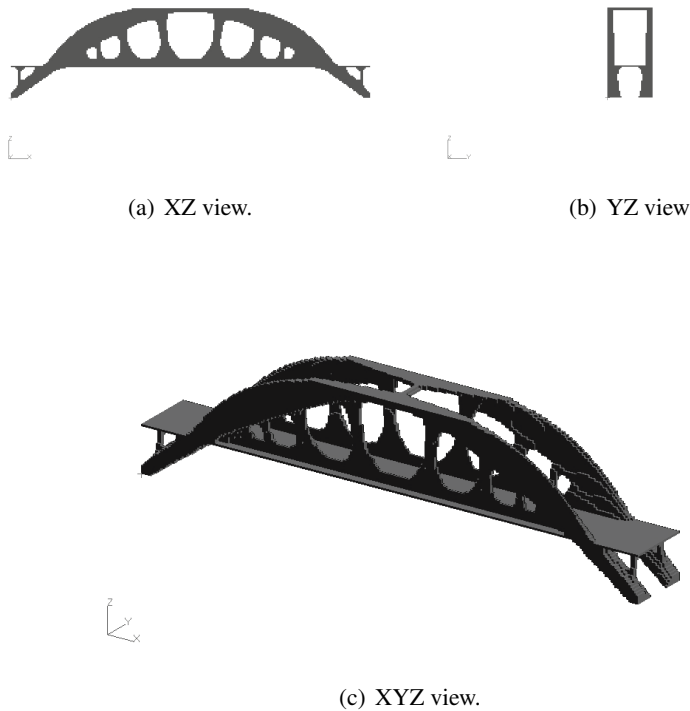


Figure 9: Optimal 3D topology of compression bridge.

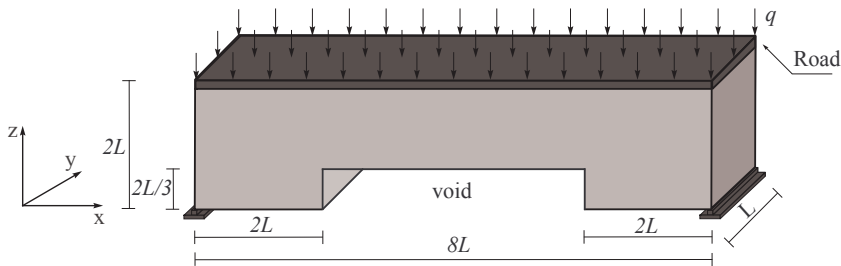


Figure 10: Arch bridge domain.

### 5.3 Example 3

The problem definition is similar to the previous example, except that the deck is located at the top of the cuboid structure. The bridge structure is simply supported

at the lower outer left and right edges, with a uniformly distributed traffic loading applied at the top surface as shown in Fig. 10. The void volume should allow passage of boats under the bridge.



Figure 11: Optimal 2D topology of arch bridge.

The MG design algorithm is run on a  $257 \times 65$  cells for the two-dimensional case and  $257 \times 65 \times 33$  cells for the three-dimensional case. The two-dimensional converged design for a Poisson ratio  $\nu = 0.3$  and a volume fraction  $\eta = 0.15$  is shown in Fig. 11. The converged topology corresponds to a compression arch that supports the deck by means of compression members. The two-dimensional final topology is shown in Fig. 11. Its layout is similar to that of the XZ view of the final three-dimensional topology presented in Fig. 12. The converged topology in Fig. 11 requires 57 design iterations in about 21 seconds, and the topology in Fig. 12 requires 59 design updates for a run time of 2673 seconds.

## 6 Conclusion

Combined multigrid cellular automata implementations for the topology optimization of continuum structures have been presented in this work. Two design algorithms have been proposed, a multigrid and a full multigrid design algorithms. Numerical tests for a symmetric cantilever example illustrate the efficiency of the combined multigrid cellular automata design algorithm in solving the topology optimization problem compared to the use of the commercial NASTRAN code for the analysis phase. The multigrid scheme is shown to accelerate the convergence of the analysis phase and the full multigrid to improve convergence of both analysis and design in the topology optimization problem. The computational cost for the multigrid algorithms is indeed found to be proportional to the number of cells,

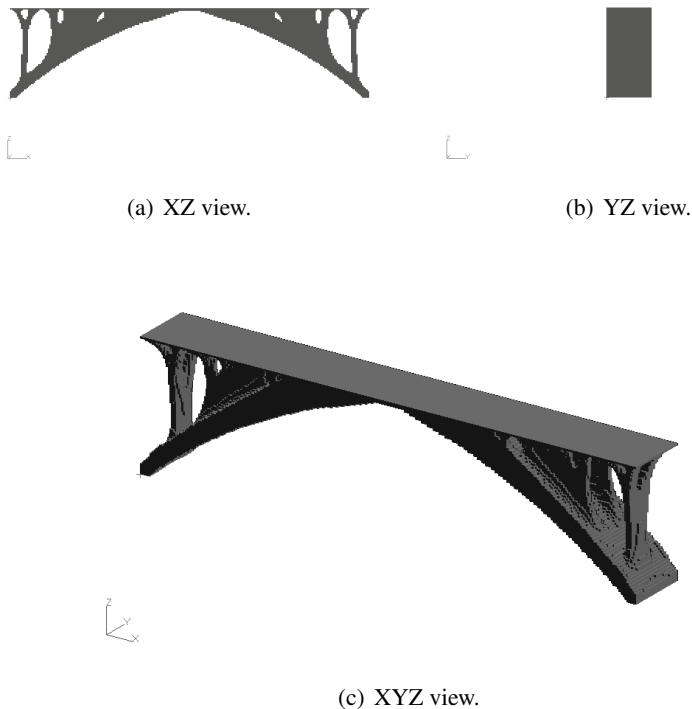


Figure 12: Optimal 3D topology of arch bridge.

that is an effort of order  $O(N)$ . Applied to 2D and 3D topology optimization of example bridge structures, the multigrid accelerated cellular automata design algorithm generates realistic topologies such as the familiar compression arch bridge architectures.

**Acknowledgement:** This research was supported by the National Science Foundation, Grant NSF OISE-0353186. The investigations are part of the Dutch INWIND project and are sponsored by SenterNovem, the Netherlands Agency for Energy and the Environment, under contract EOSLT07001.

## References

**Abdalla, M. M.; Gürdal, Z. (2002):** Structural design using optimality based cellular automata. In *43th AIAA/ASME/AHS/ASC Structures, Structural Dynamics*

and material Conference, Denver, Co.

**Abdalla, M. M.; Gürdal, Z.** (2004): Structural design using cellular automata for eigenvalue problems. *Structural and Multidisciplinary Optimization*, vol. 26, pp. 200–208.

**Beckers, M.** (1999): Topology optimization using a dual method with discrete variables. *Structural Optimization*, vol. 17, pp. 14–24.

**Bendsøe, M. P.** (1989): Optimal shape design as a material distribution problem. *Structural and Multidisciplinary Optimization*, vol. 1, pp. 193–200.

**Bendsøe, M. P.; Kikuchi, N.** (1988): Generating optimal topologies in structural design using homogenization method. *Computer Methods in Applied Mechanics and Engineering*, vol. 71, pp. 197–224.

**Cisilino, A. P.** (2006): Topology Optimization of 2D Potential Problems Using Boundary Elements. *CMES: Computer Modeling in Engineering & Sciences*, vol. 15, no. 2, pp. 99–106.

**Dreyer, T.; Maar, B.; Schulz, V.** (2000): Multigrid optimization in application. *Journal of Computational and Applied Mathematics*, vol. 120, pp. 67–84.

**Gürdal, Z.; Tatting, B.** (2000): Cellular automata for design of truss structures with linear and non linear response. In *41st AIAA/ASME/ASCE/AHS/ASC Structures, Structural Dynamics and Materials Conference, Atlanta, GA*.

**Hackbush, W.** (1985): *Multigrid methods and applications*. Springer.

**Juan, Z.; Shuyao, L.; Yuanbo, X.; Guangyao, L.** (2008): A Topology Optimization Design for the Continuum Structure Based on the Meshless Numerical Technique. *CMES: Computer Modeling in Engineering & Sciences*, vol. 34, no. 2, pp. 137–154.

**Kim, S.; Abdalla, M. M.; Gürdal, Z.; Jones, M.** (2004): Multigrid accelerated cellular automata for structural design optimization: A 1-D implementation. In *45th AIAA/ASME/ASCE/AHS/ASC Structures, Structural Dynamics and Materials Conference, Palm Springs, California*.

**Kim, Y. Y.; Yoon, G. H.** (2000): Multi-resolution multi-scale topology optimization - a new paradigm. *International Journal of Solids and Structures*, vol. 37, pp. 5529–5559.

**Kita, E.; Toyoda, T.** (2000): Structural design using cellular automata. *Structural and Multidisciplinary Optimization*, vol. 19, pp. 64–73.

**Kwon, K.; Kim, J. E.; Jang, G. W.; Kim, Y. Y.** (2002): Multigrid approach for efficient integrated multiscale analysis and design optimization. In *9th AIAA/ISSMO Symposium on Multidisciplinary Analysis and Optimization*.

**Li, S.; Atluri, S. N.** (2008): The MLPG Mixed Collocation Method for Material Orientation and Topology Optimization of Anisotropic Solids and Structures. *CMES: Computer Modeling in Engineering & Sciences*, vol. 30, no. 1, pp. 37–56.

**Li, S.; Atluri, S. N.** (2008): Topology-optimization of Structures Based on the MLPG Mixed Collocation Method. *CMES: Computer Modeling in Engineering & Sciences*, vol. 26, no. 1, pp. 61–74.

**Liu, G. R.; Gu, Y. T.** (2001): A point interpolation method for two-dimensional solids. *International Journal for Numerical Methods in Engineering*, vol. 50, pp. 937–951.

**Maar, B.; Schulz, V.** (2000): Interior point multigrid methods for topology optimization. *Mathematical and Computer Modelling*, vol. 19, pp. 214–224.

**Setoodeh, S.; Abdalla, M. M.; Gürdal, Z.** (2005): Combined topology and fiber path design of composite layers using cellular automata. *Structural and Multidisciplinary Optimization*, vol. 30, pp. 413–421.

**Setoodeh, S.; Adams, D. B.; Gürdal, Z.; Watson, L. T.** (2006): Pipeline implementation of cellular automata for structural design on message-passing multiprocessors. *Mathematical and Computer Modelling*, vol. 43, pp. 966–975.

**Slotta, D. J.; Tatting, B.; Watson, L. T.; Gürdal, Z.; Missoum, S.** (2002): Convergence analysis for cellular automata applied to truss design. *Engineering Computations*, vol. 19, pp. 953–969.

**Tatting, B.; Gürdal, Z.** (2003): Cellular automata for design of two-dimensional continuum structures. In *8th AIAA/USAF/NASA/ISSMO Symposium on Multidisciplinary Analysis and Optimization, Long Beach*.

**Wang, M. Y.; Wang, X.** (2006): Structural Shape and Topology Optimization Using an Implicit Free Boundary Parametrization METHOD. *CMES: Computer Modeling in Engineering & Sciences*, vol. 13, no. 2, pp. 119–147.

**Wesseling, P.** (1992): *An introduction to multigrid methods*. Wiley.

**Xie, Y. M.; Steven, G. P.** (1993): A simple evolutionary procedure for structural optimization. *Computers and Structures*, vol. 49, pp. 885–896.



**Zakhama, R.; Abdalla, M. M.; Smaoui, H.; Gürdal, Z.** (2006): Topology design of geometrically nonlinear 2D elastic continua using CA and an equivalent truss model. In *11th AIAA/ISSMO Symposium on Multidisciplinary Analysis and Optimization*.

**Zakhama, R.; Abdalla, M. M.; Smaoui, H.; Gürdal, Z.** (2007): Multigrid implementation of cellular automata for topology optimization. In *First International Conference on Multidisciplinary Design and Applications, Besançon, France*.

**Zhou, S.; Wang, M. Y.** (2006): 3D Multi-Material Structural Topology Optimization with the Generalized Cahn-Hilliard Equations. *CMES: Computer Modeling in Engineering & Sciences*, vol. 16, no. 2, pp. 83–101.

